Sensors and Actuators B 216 (2015) 337–342

Contents lists available at ScienceDirect

Sensors and Actuators B: Chemical

journal homepage: www.elsevier.com/locate/snb

# $TiO_2$ and shrink induced tunable nano self-assembled graphene composites for label free biosensors

Peng Li[a,b], Bo Zhang[b], Tianhong Cui[b,*]

[a] State Key Laboratory of Precision Measurement Technology and Instruments, Department of Precision Instruments, Tsinghua University, Beijing 100084, China
[b] Department of Mechanical Engineering, University of Minnesota, Minneapolis, MN 55455, USA

ARTICLE INFO

*Article history:*
Received 6 February 2015
Received in revised form 24 March 2015
Accepted 30 March 2015
Available online 16 April 2015

*Keywords:*
Graphene
Biosensor
Self-assembly
Shrink polymer
$TiO_2$

ABSTRACT

This paper presents a simple and low cost fabrication method to derive tunable graphene composites. We used self-assembly technique to deposit graphene nanoplatelets, and used $TiO_2$ nanoparticles and shrink polymer to tune the film. Compared with conventional graphene composites which properties are fixed, this proposed graphene composites are tunable and controllable on its wetting ability (from ultra-hydrophobic to ultra-hydrophilic) and electrical properties, even after synthesis processes. Significant improvement of the performances of biosensors based on the new graphene composites was observed. The heat shrink enhances the output signal of the biosensor, and the sensitivity of the sensor grows with the $TiO_2$ nanoparticles. Biosensor based on the new graphene composites is able to detect different types of lung cancer biomarkers with superb detection limit and specificity.



## 1. Introduction

Graphene, a two-dimensional honeycomb crystal of $sp^2$-bonded carbon atoms [1], has drawn significant attention in both fundamental and applied research fields, owing to its extraordinary electrical, mechanical, and chemical properties. Graphene's extremely high carrier mobility [2,3] and thermal conductivity [4,5] make it an excellent candidate for next generation electronic applications [6–8]. Its gigantic Young's modulus [9], and breaking strength [10] make it an excellent candidate for NEMS (nanoelectromechanical systems) [11–17]. In order to extend these superb properties to macroscopic applications, manipulation of both large-scale film and integration of individual graphene nanoplatelets are required to achieve advanced multifunctional structures.

Graphene nanoplatelets have been integrated with other materials to obtain various structures [18–20]. However, the properties of these integrated graphene materials are not tunable or controllable due to their synthesis processes and fixed structure [21]. Two factors mainly determine the properties of material, components and morphology. Here we used shape memory polymer Polyolefins (PO) to control its morphology, and $TiO_2$ nanoparticles to tune the components of the material. This proposed new graphene composites are tunable and controllable on its wetting ability (from ultra-hydrophobic to ultra-hydrophilic) and electrical properties even after synthesis processes. The performances of biosensors based on the new graphene composites can also be tunable. Heat shrink increases the output signal of the sensor, and $TiO_2$ layer enhances its sensitivity. The biosensor based on the new graphene composites can realize multiplex lung cancer tumor marker detection with superb detection limit and specificity.

## 2. Experimental details, results and discussion

### 2.1. Materials

0.1% Poly-l-lysine (PLL) was received from Sigma–Aldrich Inc. without further treatments. 3% bovine serum albumin (BSA) was purchased from Sigma–Aldrich Inc. Lung cancer bio markers (both antibody and antigen), and poly (diallyldimethylammonium chloride) (PDDA) were received from Sigma–Aldrich Inc. PO shrink film was purchased from Sealed Air. Graphene solution (PureSheets MONO, 0.25 mg/ml) was received from Nanointegris.

### 2.2. Self-assembly graphene composites

The synthesis process of the new graphene composite is demonstrated in Fig. 1. A silicon mode was placed on top of PO shrink polymer, and hot embossing was applied to form micro channel

* Corresponding author. Tel.: +1 612 626 1636.
*E-mail address:* tcui@me.umn.edu (T. Cui).

http://dx.doi.org/10.1016/j.snb.2015.03.111
0925-4005/

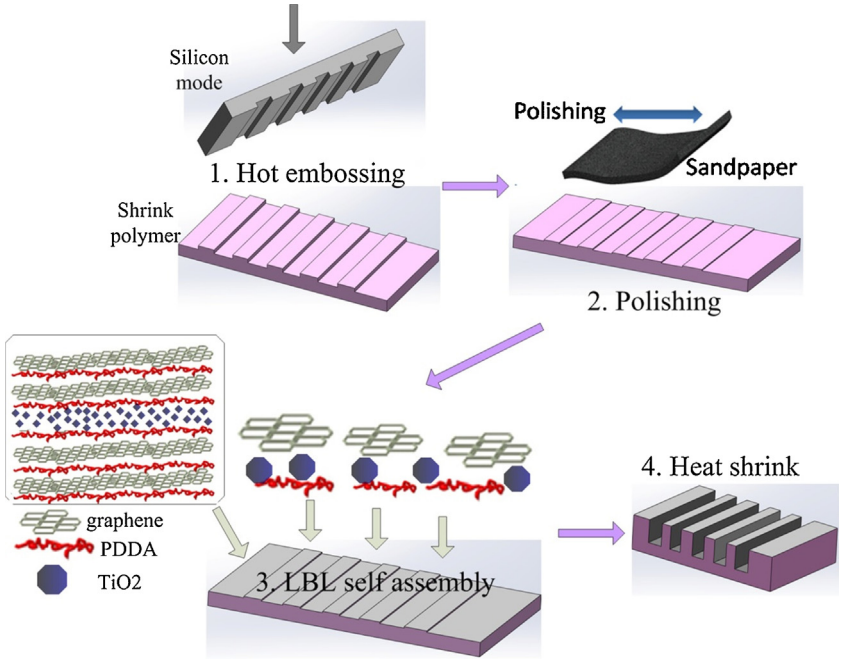


**Fig. 1.** Schematic illustration of fabrication processes of the shrink induced LBL graphene with high aspect ratio 3D channel structures. Schematic illustration of $TiO_2$ doped LBL graphene.

arrays on shrink film with high pressure of about $2 \times 10^7$ Pa for 5 min. The temperature of the hot embossing was below 90 °C in order to make sure that the PO film did not shrink during this process. After that, parallel shallow channel arrays were observed on PO surface (Fig. 2a), which were identical to the patterns on silicon mode. Next, these patterns were carefully removed by sand paper polishing, and were inspected by microscope. Then graphene nanoplatelets were layer by layer (LBL) self-assembled on the pre-treated PO polymer substrate with a sequence of $[PDDA + graphene]_2 + [PDDA + TiO_2] + [PDDA + graphene]_2$. We immersed the PO substrate into positively charged PDDA solution and negatively charged graphene solution for 10 min, respectively, and then rinsed it with DI water and blew dry it with nitrogen. The $TiO_2$ nano particles were coated on the sample by merging it in mixed solution of 1:1 0.8 M $H_3BO_3$ (Boric acid) and 0.2 M $(NH_4)_2TiF_6$ (ammonium hexafluorotitanate) at 60 °C. Longer deposition duration resulted in thicker $TiO_2$ layer (Fig. 3b). The thickness of $TiO_2$ layer was measured by P16 profilometer and atomic force microscope (AFM). Fig. 3c is AFM image of graphene nanoplatelets. The size of graphene nanoplatelets is about 150 nm. LBL graphene was characterized by a Witec Alpha300R Confocal Raman microscope with excitation laser wavelength of 514 nm, and the power of the laser is below 6 mW to avoid sample damage. Fig. 3d shows the Raman spectrum of LBL graphene. The G peak (~1580 $cm^{-1}$) and 2D peak (~2680 $cm^{-1}$) of graphene are due to doubly degenerate zone center $E_{2g}$ mode and the second order of zone-boundary phonons [5]. The large D peak (~1350 $cm^{-1}$) is cause by the edge defect of the graphene nanoplatelets. The PO coated with graphene composite was heated to desired temperature for shrinking. The film started to show obvious shrink over 100 °C. Since the shape memory material PO intended to restore to its initial place during heating, as a result, high aspect ratio micro channel arrays were generated (Fig. 2b).

### 2.3. Tunable properties of new graphene composite

The wetting ability of the new graphene composite is tunable. Wetting ability can be reflected by surface water contact angle. Small water contact angle indicates hydrophilic surface with relatively large surface energy. The contact angle for $TiO_2$, graphene,

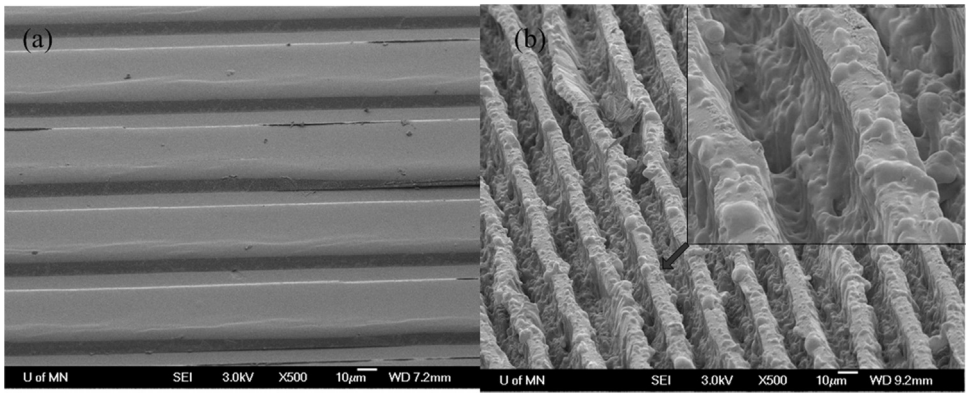


**Fig. 2.** (a) SEM image of micro channel arrays on PO after hot embossing before sand paper polishing. (b) SEM image of micro channels with high aspect ratio on PO surface after heat shrink. The inset is the zoom in view.

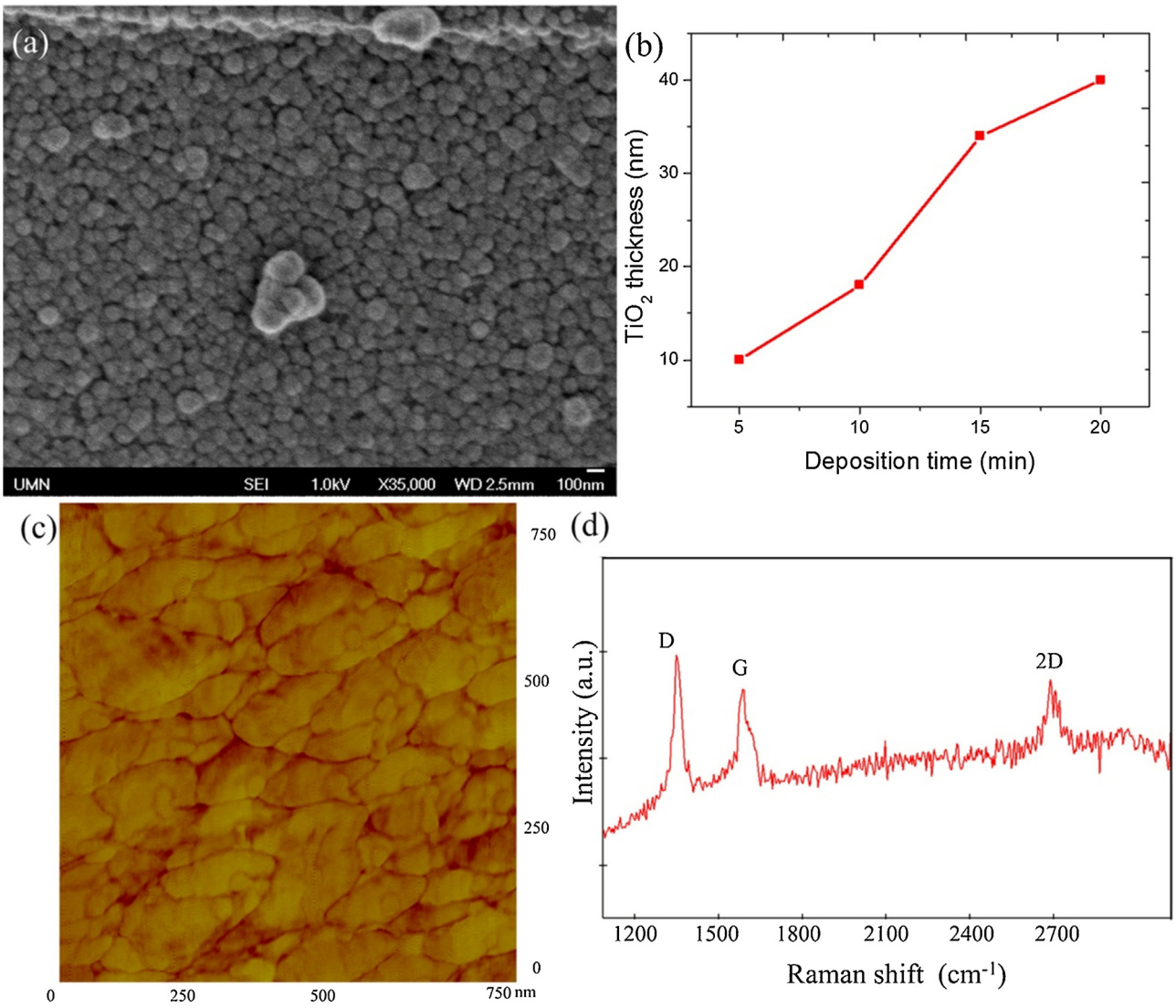


**Fig. 3.** (a) SEM image of $TiO_2$ nano particles on PO surface. (b) The thickness of the $TiO_2$ layer versus deposition duration. Longer deposition duration results in thicker $TiO_2$ layer. (c) AFM topographic image of LBL graphene. (d) Raman spectrum of LBL graphene.

and bare polymer was 0°, 70°, and 100°, respectively. $TiO_2$ layer is hydrophilic [22]. Although it is in the center of the "sandwich" structure, it affects the film's wetting ability significantly, because of LBL graphene's porous structure. The graphene composite with $TiO_2$ is more hydrophilic than pure PDDA/graphene LBL film. Besides, the wetting ability can be tuned by the thickness of $TiO_2$. Thicker $TiO_2$ layer is corresponding to smaller contact angle, indicating more hydrophilic (Fig. 4). With 3D structures, LBL graphene composite became ultra-hydrophobic, and the contact angle can be controlled by the heat shrink temperature. It is not the surface materials but the morphology is important in reaching the ultra-hydrophobic feature. Higher temperature resulted in larger contact angle and more hydrophobic surface (Fig. 4). Therefore, by adjusting the $TiO_2$ layer thickness and shrink temperature, we are able to tune the graphene composite from ultra-hydrophilic to ultra-hydrophobic which is expected to offer more controllable applications in micro fluidic field.

In addition to wetting ability, the electrical properties of the new graphene composite can also be tunable and controllable. When the material acts as the functional part of a sensor or electrical device, its conductivity is essential for the device's performances.

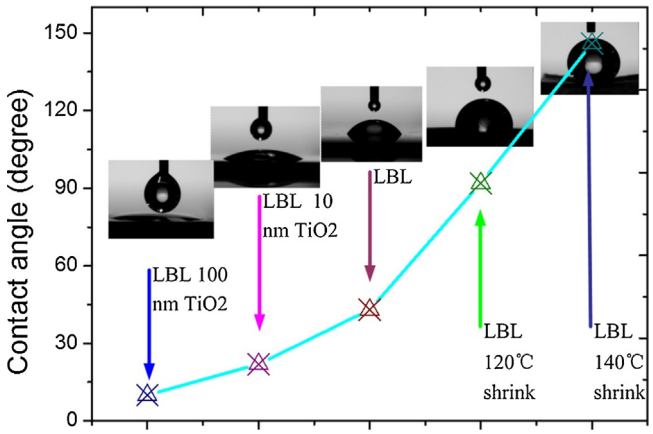


**Fig. 4.** Wetting ability of LBL graphene with $TiO_2$ layer and heat shrink. $TiO_2$ layer decreases the water contact angle (hydrophilic), while shrink induced 3D structures makes LBL graphene film more hydrophobic.

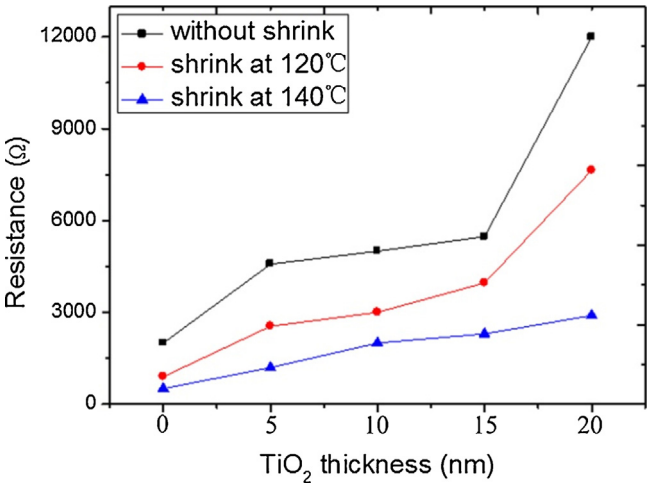


**Fig. 5.** $TiO_2$ layer increases the resistance of the LBL graphene film. Shrink induce 3D structures decreases the resistance. The electrical properties of LBL graphene can be tuned by the $TiO_2$ layer thickness or shrink temperature.

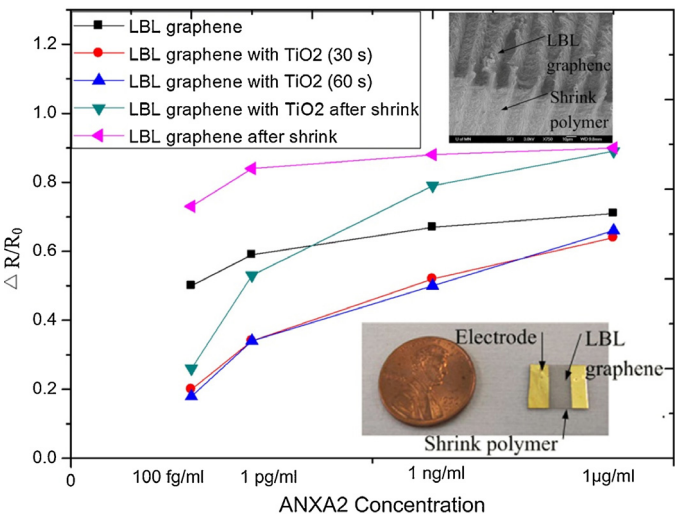


**Fig. 6.** LBL graphene lung cancer biosensor measurement. Shrink induced 3D structures increases $\Delta R/R_0$, and $TiO_2$ layer improves the sensitivity of the sensor. The insets are SEM image and optical image of graphene sensor, respectively.

We measured the resistance of the new graphene composite between two metal electrodes. With $TiO_2$ layer, the resistance of LBL graphene film significantly increased because $TiO_2$, which conductivity is much worse than graphene, enlarged the distance between graphene layers above and beneath it, and largely reduced the connection between graphene nanoplatelets. Thicker $TO_2$ layer results in larger resistance. On the contrary, the 3D channel array structures due to heat shrink intend to reduce the resistance of the film, inasmuch as it induced more connections between adjacent graphene nanoplatelets (Fig. 5). Therefore, the resistance of the film can be tuned by $TiO_2$ thickness and heat shrink temperature.

We further investigated the properties of the new graphene composites in the applications of label free bio-sensing. The graphene sensors were used to detect lung cancer tumor markers. Tumor markers are small biological molecules exists in human blood and tissue, and their high level of concentrations indicates certain cancers are very likely to present inside the human body. Therefore, tumor marker detection is very critical in disease prediction, diagnosis, especially in cancer treatment monitoring. The graphene sensor was immersed into 0.1% positive charged PLL aqueous solution for 2 h, which can enhance the immobilization of antibodies. Then the sensor was incubated for overnight at 4 °C in lung cancer bio marker capture antibody solution at a concentration of 6 μg/ml. Sequentially, it was incubated in a 3% BSA blocking solution at room temperature for 5 h to block nonspecific binding sites and improve the specificity of the sensor. After the immobilization process, the graphene sensor was ready for detection. This label-free lung cancer biosensor is low cost and easy to operate. It was characterized by measuring LBL graphene film resistance shift according to different concentrations of biomarkers. The resistances of the devices were monitored using Agilent Data Logger (34970A, Agilent Inc.). Three important lung cancer biomarkers, ANXA2, ENO1, and VEGF, were investigated.

Four different concentrations of ANXA2 antigen were detected (Fig. 6). The sensor exhibited large detection range from 100 fg/ml to 1 μg/ml. Tumor markers with higher concentration generally resulted in larger resistance shift of the sensor. It is evident that the absorption of molecules or ions by the bio-receptors on the surface of graphene can cause the change in density and mobility of charge carriers of the film, resulting in different graphene resistance values. The equation, $\rho = \frac{1}{nq\mu}$, shows this relation clearly, where $\rho$ is resistance, $n$ is carrier density, $q$ is charge per carrier, and $\mu$ is carrier mobility. 3D nano structure after heat shrink enlarged the surface area of the sensor. More molecules could be absorbed by the bio-receptors, increasing its output signal. Therefore, we observed that the sample after heat shrink dramatically increased $\Delta R/R_0$ (pink curve), which makes the detection of biomarker with low concentration easier. With $TiO_2$ layer, $\Delta R/R_0$ largely reduced in low concentration region (red and blue curve). We assume the scattering from $TiO_2$ layer, which can reduce the carrier mobility of graphene, is mainly responsible for this phenomenon. However, $\Delta R/R_0$ reduced much less in high concentration region. As a result, $TiO_2$ layer increased the slope of the curve (red and blue curve), indicating improved sensitivity of graphene sensor. Therefore, the output signal and the sensitivity of the sensor based on the new graphene composite can be tuned and enhanced by heat shrink and $TiO_2$ nano particles.

The detection limit is generally defined as three times the standard deviation of the noise [23]. The output signal $\Delta R/R_0$ of our sensor in 100 fg/ml ANXA2 antigen solution was larger than three times the standard deviation of the noise (Fig. 7a). Therefore, biosensor based on the new graphene composite can reach very low concentration: 100 fg/ml. Tumor marker detection techniques need to give accurate values for every measurement below μg/ml. The detection limit of our sensor is seven orders better than clinic requirement. In the very early stage of cancer, biomarkers emerge in human body, but their concentrations are much lower than that in a patient. Therefore, detecting extremely low concentration of biomarkers is very important to cancer prediction. Additionally, superb detection limit is important to understand cellular processes and to search for new protein biomarkers.

Specificity is critical for biosensors to identify each tumor marker correctly and reduce the chance of misleading during diagnosis process. We applied sensors immobilized with ANXA2 antibody to ENO1 and VEGF antigen detection. Their resistance shifts were smaller than 1/2 of that to ANXA2 antigen in low concentration region, and the value reduced to 1/3 in high concentration region (Fig. 7b). Similar results were observed for sensors immobilized with ENO1 or VEGF antibody (Fig. 7c and d). Therefore, sensors only have prominent response to corresponding antigen, indicating good specificity of our graphene sensors.

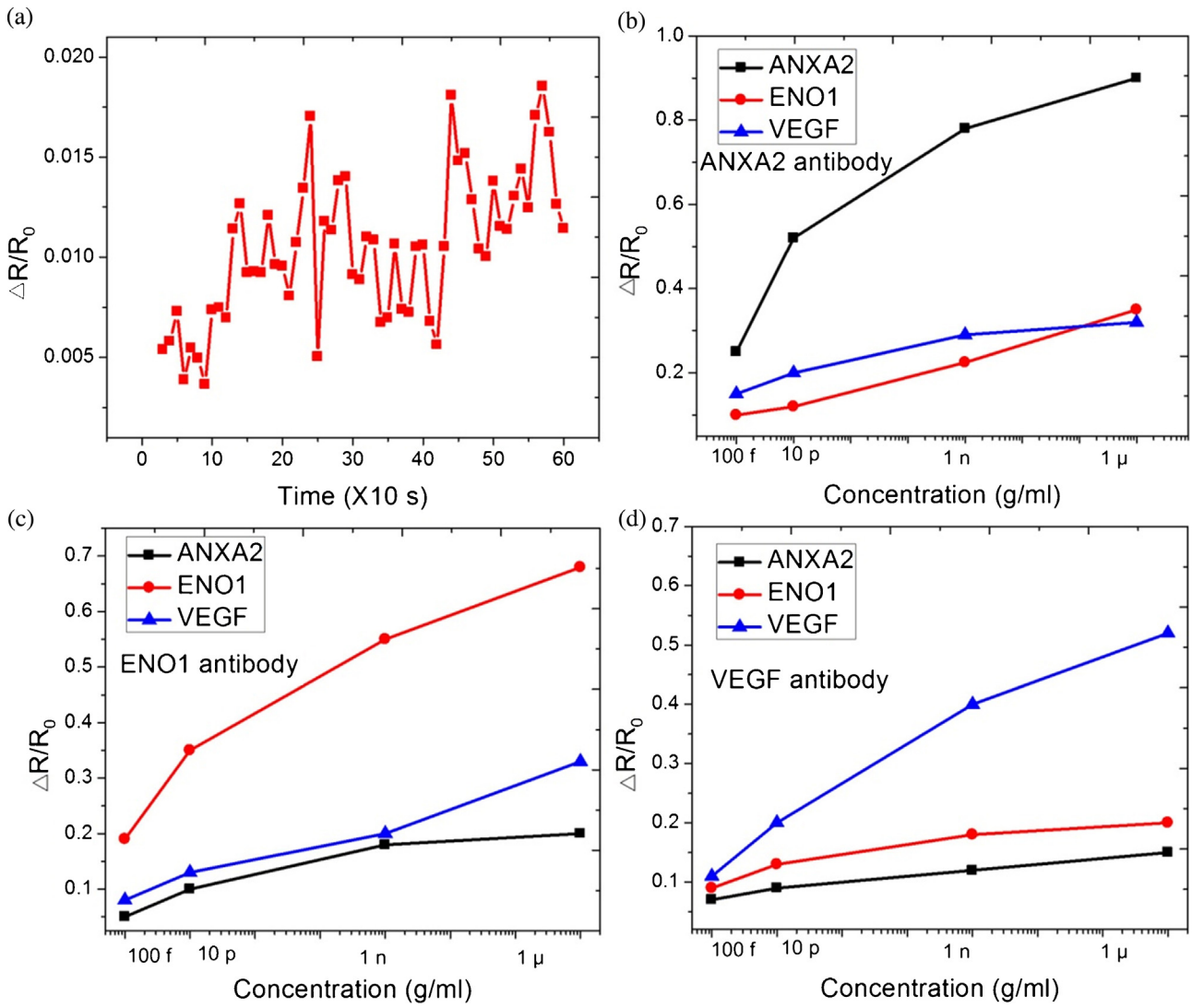


**Fig. 7.** (a) Noise of graphene biosensor during tumor marker detection which is smaller than 0.02 $\Delta R/R_0$. (b–d) Specificity of the graphene sensor. (b) Graphene sensors with ANXA2 antibody only have prominent response to ANXA2 antigen. (c) Graphene sensors with ENO1 antibody only have prominent response to ENO1 antigen. (d) Graphene sensors with VEGF antibody only have prominent response to VEGF antigen.

## 3. Conclusion

We developed a simple and low cost approach to fabricate tunable self-assembly graphene composites. $TiO_2$ nanoparticles and shrink polymer PO were applied to tune and control the film's wetting ability and electrical properties even after synthesis processes. We can also tune and control the performances of the lung cancer biosensors based on this new graphene composites. The heat shrink increases the resistance shift of the sensor, and the sensitivity of the sensor increases with the $TiO_2$ layer. The tunable graphene composite is expected to offer more controllable and flexible applications in chemical, biological detection and micro-fluidic with simple and low cost strategy.

## Acknowledgement

The authors acknowledge the assistance of fabrication and characterization from Minnesota Nano Center and Characterization Facility at the University of Minnesota.

## References

[1] K.S. Novoselov, A.K. Geim, S.V. Morozov, D. Jiang, Y. Zhang, S.V. Dubonos, I.V. Grigorieva, A.A. Firsov, Electric field effect in atomically thin carbon films, Science 306 (2004) 666–669.
[2] X. Du, I. Skachko, A. Barker, E.Y. Andrei, Approaching ballistic transport in suspended graphene, Nat. Nanotechnol. 3 (2008) 491–495.
[3] B.Y. Chen, H.X. Huang, X.M. Ma, L. Huang, Z.Y. Zhang, L.M. Peng, How good can CVD-grown monolayer graphene be? Nanoscale 6 (2014) 15255–15261.
[4] A.A. Balandin, S. Ghosh, W. Bao, I. Calizo, D. Teweldebrhan, F. Miao, C.N. Lau, Superior thermal conductivity of single-layer graphene, Nano Lett. 8 (2008) 902–907.
[5] F. Giorgia, C. Andrea, P. Lorenzo, L. Michele, M. Nicola, M. Francesco, Thermal conductivity of graphene and graphite: collective excitations and mean free paths, Nano Lett. 14 (2014) 6109–6114.
[6] X. Liang, Z. Fu, S.Y. Chou, Graphene transistors fabricated via transfer-printing in device active-areas on large wafer, Nano Lett. 7 (2007) 3840–3844.
[7] L. Song, L. Ci, W. Gao, P.M. Ajayan, Transfer printing of graphene using gold film, ACS Nano 3 (2009) 1353–1356.
[8] S. Jang, E. Hwang, J.H. Cho, Graphene nano-floating gate transistor memory on plastic, Nanoscale 6 (2014) 15286–15292.
[9] C. Lee, X. Wei, J.W. Kysar, J. Hone, Measurement of the elastic properties and intrinsic strength of monolayer graphene, Science 321 (2008) 385–388.
[10] G.H. Lee, R.C. Cooper, S.J. An, S. Lee, A. van der Zande, N. Petrone, A.G. Hammerberg, C. Lee, B. Crawford, W. Oliver, J.W. Kysar, J. Hone, High-strength

chemical-vapor-deposited graphene and grain boundaries, Science 340 (2013) 1073–1076.
[11] C. Gomez-Navarro, M. Burghard, K. Kern, Elastic properties of chemically derived single graphene sheets, Nano Lett. 8 (2008) 2045–2049.
[12] C. Chen, S. Rosenblatt, K.I. Bolotin, W. Kalb, P. Kim, I. Kymissis, H.L. Stormer, T.F. Heinz, J. Hone, Performance of monolayer graphene nanomechanical resonators with electrical readout, Nat. Nanotechnol. 4 (2009) 861–867.
[13] P. Weber, J. Guttinger, I. Tsioutsios, D.E. Chang, A.B. Achtold, Coupling graphene mechanical resonators to superconducting microwave cavities, Nano Lett. 14 (2014) 2854–2860.
[14] J.W. Wang, B.S. Wang, H.S. Park, T. Rabczuk, Adsorbate migration effects on continuous and discontinuous temperature-dependent transitions in the quality factors of graphene nanoresonators, Nanotechnology 25 (2014) 025501.
[15] S. Shivaraman, R.A. Barton, X. Yu, J. Alden, L. Herman, M. Chandrashekhar, J. Park, L. McEuen, J.M. Parpia, H.G. Craihead, M.G. Spencer, Free-standing epitaxial graphene, Nano Lett. 9 (2009) 3100–3105.
[16] P. Li, G. Jing, B. Zhang, S. Sando, T. Cui, Single-crystalline monolayer and multilayer graphene nano switches, Appl. Phys. Lett. 104 (2014)113110.
[17] P. Li, G. Jing, B. Zhang, S. Sando, T. Cui, Wafer-size free-standing single-crystalline graphene device arrays, Appl. Phys. Lett. 105 (2014) 083118.
[18] B. Zhang, Q. Li, T. Cui, Ultra-sensitive suspended graphene nanocomposite cancer sensors with strong suppression of electrical noise, Biosens. Bioelectron. 31 (2012) 105–109.
[19] Z. Wang, S. Eigler, M. Halik, Scalable self-assembled reduced graphene oxide transistors on flexible substrate, Appl. Phys. Lett. 104 (2014) 243502.
[20] N. Cernetic, S.F. Wu, J.A. Davies, B.W. Krueger, D.O. Hutchins, X.D. Xu, H. Ma, A.K.Y. Jen, Systematic doping control of CVD graphene transistors with functionalized aromatic self-assembled monolayers, Adv. Funct. Mater. 24 (2014) 3464–3470.
[21] B. Ahmadi-Moghadam, M. Sharafimasooleh, S. Shadlou, F. Taheri, Effect of functionalization of graphene nanoplatelets on the mechanical response of graphene/epoxy composites, Mater. Des. 66 (2014) 142–149.
[22] E.R. Negeed, M. Albeirutty, Y. Takata, Dynamic behavior of micrometric single water droplets impacting onto heated surfaces with $TiO_2$ hydrophilic coating, Int. J. Therm. Sci. 79 (2014) 1–17.
[23] E. Pretsch, The new wave of ion-selective electrodes, TrAC, Trends Anal. Chem. 26 (2007) 46–51.

## Biographies

**Peng Li** received B.S. degree in Electronic Engineering from Tianjin University, China, in 2007, and Ph. D. degree in Precision Instruments from Tsinghua University, China, in 2012. He is currently working in Department of Mechanical engineering at Tsinghua University. His current research interests include graphene material synthesis, and graphene NEMS device fabrication and their application in actuators and sensors.

**Bo Zhang** received B.S. degree in Department of Precision Instruments from Tsinghua University in 2009, and Ph.D. degree in Department of Mechanical Engineering from the University of Minnesota in 2014. His current research interests include micro sensors for biomedical and biological applications.

**Tianhong Cui** is currently a Professor of Mechanical Engineering and an Affiliate Senior Member of the graduate faculty in Department of Electrical and Computer Engineering and Department of Biomedical Engineering at the University of Minnesota. He joined the faculty of the University of Minnesota in 2003. From 1995 to 2003, he held research or faculty positions at Tsinghua University, University of Minnesota, National Laboratory of Metrology in Japan, and Louisiana Tech University, respectively. His current research interests include MEMS/NEMS and nanotechnology for medical applications. He published more than 240 technical papers in the above area. He is serving as an associate editor for Journal of Nanoscience and Nanotechnology, and Journal of Nano Research. He is also an Executive Editor-in-Chief for two Nature journals, Light: Science & Applications and Microsystems & Nanoengineering.